



Analytic Approach to non-Newtonian Jeffery Fluid Flow in a Catheterized Curved Artery: Exploring the Impact of Heat, Mass Transfer and Magnetic Field

Gauri Sethi¹ , Surendra Kumar Agarwal^{1*} 

Abstract

This investigation analyzes the physical properties of blood flow via a catheter in a damaged, curved artery while taking mass and heat transfer in a magnetic field. In order to get analytical answers for axial velocity, temperature, and concentration, this study models and solves the set of equations for the incompressible, non-Newtonian Jeffrey fluid under the mild stenosis approximation. The findings show that while there is less barrier to blood flow and concentration, an increase in the parameter of curvature raises shear stress of the artery wall, blood velocity, and temperature. The effect on key factors such as axial velocity, flow rate, resistance impedance, and wall shear stress of arterial geometrical variables such as stenosis, slip parameter, Hartmann number, and catheter parameter is thoroughly and quantitatively analyzed. Moreover, in trapping phenomena, the artery's curvature throws off the symmetry of the trapped bolus.

Keywords: Artery wall, Blood flow, Heat-mass transfer, Jeffery fluid, Magnetic field

2020 AMS: 34B15, 76D05, 76W05

¹ Department of Mathematics, Inspiration Innovation Synergy University, India, gaurisethi36320@iisuniv.ac.in, surendrakumar.agarwal@iisuniv.ac.in 

*Corresponding author

Received: 20 December 2024, **Accepted:** 01 June 2025, **Available online:** 14 June 2025

How to cite this article: G. Sethi, S. K. Agarwal *Analytic approach to non-Newtonian Jeffery fluid flow in a catheterized curved artery: Exploring the impact of heat, mass transfer and magnetic field*, Commun. Adv. Math. Sci., 8(2) (2025), 86-99.

1. Introduction

These days, no general analytic approaches are accessible for the integration of the Navier-Stokes equations. Moreover, solutions are applicable to all viscosity values, although they are only known for special cases [1]. The cardiovascular system maintains blood flowing convectively through the body's many organs. A serious condition known as atherosclerosis, sometimes referred to as artery stenosis, is brought on by the blood flow's deviation from its typical state [2], [3]. A number of arterial illnesses, including myocardial infarction, artery disease, renal disease, thrombosis, high blood pressure, and strokes, can be brought on by stenosis at one or more key places [4]. When a catheter is placed inside an artery, it modifies the hemodynamic properties and flow pattern. A few theoretical and experimental works examined blood circulation in curved arteries with stenosis. Via mathematical research, Dash et al. (1999) [5] investigated the flow of fluid theory through an intravenous bend an artery stenotic. Blood is modeled as an incompressible Newtonian fluid with a laminar propagation that is supposed to be constant. In his work, the problem-solving analytical method where the resulting boundary conditions were used to solve the governing equations for the predicted model, and the analytic method yielded closed-form solutions for temperature, velocity,

and slip velocity.

These days, it is generally accepted that magnetic fields can be used in physiotherapy. With the use of magnetic force, many people are being healed by regulating blood flow and temperature. This model took into account the axis-symmetric blood flow in a bending channel with aberrant growth of stenosis. The moderate stenosis situation has been used to simulate the constitutive equations for an incompressible and steady non-Newtonian tangent hyperbolic fluid. The combined outcome of variable and constant Cu-blood transportation with shape factor was investigated by Ayub et al. (2019) [6]. In this scenario, the blood flow in a bend stenotic artery with balloon is mathematically studied by gathering its behavior as a viscous fluid. Additionally, the Cu-blood medicated form in a bend artery with overlapping stenosis was examined. Using the numerical method, Zaman and Khan (2021) [7] investigated the combined effects of curvature and non-Newtonian flow on unstable nanofluid flow in a curved, overlapping stenosed link. The outcome of the study may serve as a single guideline for a pressure equation that yields a robust solution to blood flow issues. Analytical investigations pertaining to blood flow have been conducted. In the presence of a uniform magnetic field, this study investigates the irregular blood flow via a catheterized artery with overlapping stenosis while taking mass and heat transfer into account.

The comprehension and progression of vascular disorders in general depend heavily on the heat effect phenomena on blood, and the growth and development of atherogenetic processes are more strongly influenced by heat flow in conjunction with the movement of large molecules containing dissolved gases to and through the arterial wall. Research indicates that over 80 percent of deaths from heart disease are related to abnormal blood flow to and from the heart. Thin catheter tubes used in medicine that are constructed of materials of the highest caliber and have a variety of uses [8].

2016, Zaman et al. [9] investigated the unsteady flow of non-Newtonian blood through an inclined and catheterized artery with overlapping stenosis. The results reveal that both slip and inclination angle significantly affect axial velocity, flow rate, wall shear stress, and impedance. Except for wall shear stress, all parameters increase with higher slip or inclination. Hayat et al.(2007) [10] conducted a theoretical study on the peristaltic motion of a Jeffrey fluid within a circular tube, accounting for fluid compressibility and viscoelastic properties. The results reveal that backflow occurs mainly at high relaxation times and low retardation times, and the net flow oscillations in Jeffrey fluid are milder than those in Maxwell fluid.

Chakravarty and Mandal(1996) [11] developed a nonlinear two-dimensional model to study unsteady blood flow through an artery with overlapping stenosis under whole-body acceleration. The artery is modeled as an elastic tube, and blood is treated as a Newtonian fluid influenced by a pulsatile pressure gradient and arterial wall motion. Their findings highlight how body acceleration, stenosis severity, and wall elasticity affect velocity profiles and overall flow behavior during a cardiac cycle. In 2024, M. A. El Kot [12] conducts a theoretical investigation on the behavior of non-Newtonian Jeffrey fluid flowing through a curved, diseased, and catheter-inserted artery, considering the effects of heat and mass transfer. The results indicate that higher arterial curvature leads to an increase in flow velocity, wall shear stress, and temperature, while simultaneously lowering the resistance to flow and solute concentration.

The aforementioned discussions highlight the paucity of research on the mechanics of non-Newtonian blood flow and the dearth of research that considers the impact of magnetic particles, body force, and electrical force on the flow of Jeffrey fluid via a tapering artery that has stenosis in the presence of a magnetic field and wall slip condition. A mathematical model is offered here to study the combined effects of slip velocity, magnetic field, and electrical field on pertinent flow properties for non-Newtonian blood flow in a tapering stenosed artery. The governing equations of motion and energy for the nanofluid model have been determined and simplified, assuming a low Reynolds number and mild stenosis.

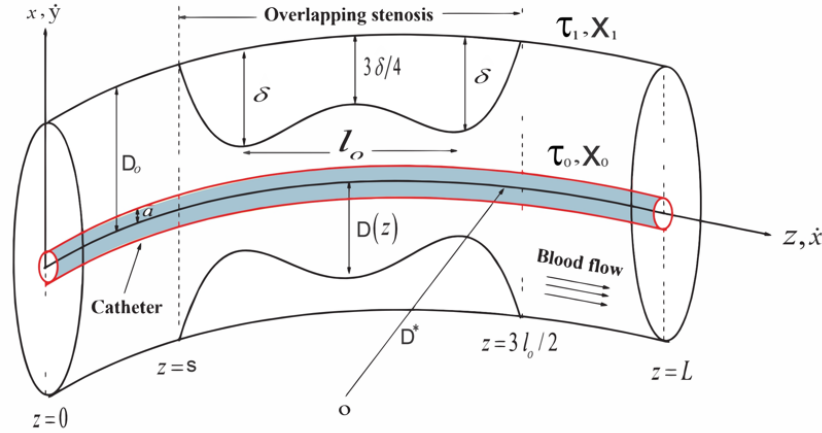
2. Problem Formulation

Let us assume that an incompressible non-Newtonian Jeffrey fluid is flowing in a cylindrically curved arterial portion of measure L , with a moderate cramping and radius D_o , wrapped inside a circle with a radius of D^* and centered at the origin o . Also consider another solid circular cylindrical flexible tube (catheter) with a radius of $\bar{a}(\ll 1)$ is inserted into the artery. \dot{y} stands for an axial direction and \dot{x} for a radial direction in the coordinate system. During the heat and mass transfer process, it is assumed that the artery wall experiences temperature τ_1 and concentration X_1 , while the catheter surface experiences temperature τ_0 and concentration X_0 , where $\tau_1 > \tau_0$ and $X_1 > X_0$.

The restricted curved region's geometric shape is taken as

$$\frac{D(z)}{D_0} = \begin{cases} 1 - \frac{\delta(z-s)}{3D_0l_0^4} [33l_0^3 - 94(z-s)l_0^2 + 96(z-s)^2l_0 - 32(z-s)^3], & \text{for } s \leq z \leq s + \frac{3l_0}{2} \\ 1, & \text{otherwise.} \end{cases}$$

The length of the conflicting stenosis is $\frac{3l_0}{2}$, where d is the position of the stenosis and D_0 is the normal blood vessel's cross sectional radius. In this case, δ represents the critical height of the stenosis, so that at $z = s + \frac{l_0}{2}$ and $z = s + l_0$, the ratio $\frac{\delta}{D_0} \ll 1$, appears. $\frac{3\delta}{4}$ is the stenosis thickness at a range from the origin of $z = s + \frac{3l_0}{4}$.



The governing equations stated here may be applied to present the problem's mathematical representation
Continuity Equation

$$\frac{1}{x} \frac{\partial}{\partial x}(x\dot{y}) + \frac{\partial \dot{x}}{\partial z} = 0 \quad (2.1)$$

Momentum Equation:

$$\rho \left[\frac{\partial \dot{y}}{\partial \xi} + \dot{y} \frac{\partial \dot{y}}{\partial x} + \frac{D^* \dot{x}}{x+D^*} \frac{\partial \dot{y}}{\partial z} - \frac{\dot{x}^2}{x+D^*} \right] = -\frac{\partial \Pi}{\partial x} + \frac{1}{x+D^*} \frac{\partial}{\partial x} [(x+D^*)S_{xx}] + \frac{D^*}{x+D^*} \frac{\partial S_{xz}}{\partial z} - \frac{\partial S_{zz}}{\partial (x+D^*)} \quad (2.2)$$

Momentum Equation

$$\rho \left[\frac{\partial \dot{x}}{\partial \xi} + \dot{y} \frac{\partial \dot{x}}{\partial x} + \frac{D^* \dot{x}}{x+D^*} \frac{\partial \dot{x}}{\partial z} + \frac{\dot{x}\dot{y}}{x+D^*} \right] = -\frac{D^*}{x+D^*} \frac{\partial \Pi}{\partial z} + \frac{1}{(x+D^*)^2} \frac{\partial}{\partial x} [(x+D^*)^2 S_{xz}] + \frac{D^*}{x+D^*} \frac{\partial S_{zz}}{\partial z} - \sigma B_0^2 \dot{x} \quad (2.3)$$

Energy Equation

$$\rho c_p \left[\frac{\partial \Theta}{\partial \xi} + \dot{y} \frac{\partial \Theta}{\partial x} + \frac{D^* \dot{x}}{x+D^*} \frac{\partial \Theta}{\partial z} \right] = \frac{K}{x+D^*} \left[\frac{\partial}{\partial x} \left((x+D^*) \frac{\partial \Theta}{\partial x} \right) + \frac{\partial}{\partial z} \left(\frac{D^{*2}}{x+D^*} \frac{\partial \Theta}{\partial z} \right) \right] + \mu \left[4 \left(\frac{\partial \dot{y}}{\partial x} \right)^2 + \left(\frac{\partial \dot{x}}{\partial x} + \frac{D^*}{x+D^*} \frac{\partial \dot{y}}{\partial z} - \frac{\dot{x}}{x+D^*} \right)^2 \right] \quad (2.4)$$

Concentration Equation

$$\left[\frac{\partial n}{\partial \xi} + \dot{y} \frac{\partial n}{\partial x} + \frac{D^* \dot{x}}{x+D^*} \frac{\partial n}{\partial z} \right] = \frac{M_d}{x+D^*} \left[\frac{\partial}{\partial x} \left((x+D^*) \frac{\partial n}{\partial x} \right) + \frac{\partial}{\partial z} \left(\frac{D^{*2}}{x+D^*} \frac{\partial n}{\partial z} \right) \right] + \frac{M_d K_\tau}{\tau_m} \frac{1}{x+D^*} \left[\frac{\partial}{\partial x} \left((x+D^*) \frac{\partial \Theta}{\partial x} \right) + \frac{\partial}{\partial z} \left(\frac{D^*}{x+D^*} \frac{\partial \Theta}{\partial z} \right) \right] \quad (2.5)$$

where X is the fluid concentration, τ is the temperature, K signifies the thermal conductivity, c_p is the specific heat at constant pressure, τ_m is the temperature of the medium, M_d is the coefficients of mass diffusivity, and K_τ is the thermal-diffusion ratio. where \dot{y} and \dot{x} are the velocity components in radial and axial directions, respectively, and Π is the fluid pressure, ρ is the fluid density, and μ is the fluid viscosity.

The constitutive equations for the Jeffery fluid are

$$S = \frac{\mu}{1+\lambda} \left(A_1 + \lambda_1 \frac{dA_1}{dt} \right),$$

where S is the additional stress tensor and The first Rivlin Ericksen tensor is $A_1 = \nabla V + (\nabla V)^T$ the transpose is indicated by T and the Jeffrey fluid parameters are λ (relaxation time) and λ_1 (retardation time).

$$\dot{y} = \dot{x} = 0, \quad \tau = \tau_0, \quad X = X_0 \quad \text{at} \quad x = a \quad (2.6)$$

$$\dot{y} = \dot{x} = 0, \quad \tau = \tau_1, \quad X = X_1 \quad \text{at} \quad x = D(z) \quad (2.7)$$

Using the following non-dimensional variable:

$$x = D_0 x', \quad z = l_0 z', \quad \dot{y} = \frac{\delta \dot{x}_0 y'}{l_0}, \quad D = D_0 D', \quad \dot{x} = \dot{x}_0 \dot{x}', \quad \xi = \frac{l_0 \xi'}{\dot{x}_0}, \quad \Pi = \frac{\dot{x}_0 l_0 \mu \Pi'}{D_0^2}, \quad (2.8)$$

$$\tau = \tau_0 + (\tau_1 - \tau_0) \Theta, \quad X = X_0 + (X_1 - X_0) n.$$

When the dashes are removed from the equations (2.1)-(2.5) using (2.6)-(2.8), the results are:

$$\delta^* \frac{\partial}{\partial x} [(x + D_c) \dot{y}] + D_c \frac{\partial \dot{x}}{\partial z} = 0 \quad (2.9)$$

$$\begin{aligned} & \frac{\rho \dot{x}_0 D_0^3}{l_0 \mu} \left[\frac{\delta}{l_0^2} \frac{\partial \dot{y}}{\partial \xi} + \frac{\delta^2}{l_0^2 D_0} \dot{y} \frac{\partial \dot{y}}{\partial x} + \frac{\delta}{l_0^2} \frac{D_c \dot{x}}{x + D_c} \frac{\partial \dot{y}}{\partial z} - \frac{1}{D_0} \frac{\dot{x}^2}{x + D_c} \right] \\ &= - \frac{\partial \Pi}{\partial x} + \frac{D_0^2}{\dot{x}_0 l_0} \frac{\delta}{\dot{x}_0 l_0} \frac{2}{1 + \lambda} \frac{1}{x + D_c} \frac{\partial}{\partial x} \left[(x + D_c) \left(1 + \lambda_1 \frac{\dot{x}_0}{l_0} \left(\frac{\delta}{D_0} \dot{y} \frac{\partial}{\partial x} + \frac{D_c \dot{x}}{x + D_c} \frac{\partial}{\partial z} \right) \right) \left(\frac{\partial \dot{y}}{\partial x} \right) \right] \\ &+ \frac{D_0^3}{\dot{x}_0 l_0^2} \frac{\dot{x}_0}{D_0} \frac{1}{1 + \lambda} \frac{D_c}{x + D_c} \frac{\partial}{\partial z} \left[\left(1 + \lambda_1 \frac{\dot{x}_0}{l_0} \left(\frac{\delta}{D_0} \dot{y} \frac{\partial}{\partial x} + \frac{D_c \dot{x}}{x + D_c} \frac{\partial}{\partial z} \right) \right) \times \left(\frac{\partial \dot{x}}{\partial x} + \frac{\delta D_0}{l_0^2} \dot{y} \frac{D_c \dot{x}}{x + D_c} \frac{\partial \dot{y}}{\partial x} - \frac{\dot{x}}{x + D_c} \right) \right] \\ &- \frac{D_0^2}{\dot{x}_0 l_0^2} \frac{\dot{x}_0}{1 + \lambda} \frac{1}{x + D_c} \left[\left(1 + \lambda_1 \frac{\dot{x}_0}{l_0} \left(\frac{\delta}{D_0} \dot{y} \frac{\partial}{\partial x} + \frac{D_c \dot{x}}{x + D_c} \frac{\partial}{\partial z} \right) \right) \times \left(\frac{\dot{x}_0}{l_0} \frac{D_c}{x + D_c} \frac{\partial \dot{y}}{\partial z} - \frac{\delta \dot{x}_0}{l_0 D_0} \frac{\dot{y}}{x + D_c} \right) \right] \\ &R_e \varepsilon \left[\frac{\delta D_0}{l_0^2} \frac{\partial \dot{y}}{\partial \xi} + \delta^* \varepsilon^2 \left(\dot{y} \frac{\partial \dot{y}}{\partial x} + \frac{D_c \dot{x}}{x + D_c} \frac{\partial \dot{y}}{\partial z} \right) - \frac{\dot{x}^2}{x + D_c} \right] = - \frac{\partial \Pi}{\partial x} \\ &+ \frac{2 \delta^* \varepsilon^2}{1 + \lambda} \frac{1}{x + D_c} \frac{\partial}{\partial x} \left[(x + D_c) \left(1 + \lambda_1^* \left(\delta^* \dot{y} \frac{\partial}{\partial x} + \frac{D_c \dot{x}}{x + D_c} \frac{\partial}{\partial z} \right) \right) \left(\frac{\partial \dot{y}}{\partial x} \right) \right] \\ &+ \frac{\varepsilon^2}{1 + \lambda} \frac{D_c}{x + D_c} \frac{\partial}{\partial z} \left[\left(1 + \lambda_1^* \left(\delta^* \dot{y} \frac{\partial}{\partial x} + \frac{D_c \dot{x}}{x + D_c} \frac{\partial}{\partial z} \right) \right) \left(\frac{\partial \dot{x}}{\partial x} + \frac{\delta^* \varepsilon^2 D_c}{x + D_c} \frac{\partial \dot{y}}{\partial z} - \frac{\dot{x}}{x + D_c} \right) \right] \\ &- \frac{2 \varepsilon^2}{1 + \lambda} \frac{1}{x + D_c} \left[\left(1 + \lambda_1^* \left(\delta^* \dot{y} \frac{\partial}{\partial x} + \frac{D_c \dot{x}}{x + D_c} \frac{\partial}{\partial z} \right) \right) \left(\frac{D_c}{x + D_c} \frac{\partial \dot{x}}{\partial z} + \frac{\delta^* \dot{y}}{x + D_c} \right) \right] \end{aligned} \quad (2.10)$$

$$\begin{aligned} & \rho \frac{\dot{x}_0 D_0^2}{l_0 \mu} \left[\frac{\partial \dot{x}}{\partial \xi} + \delta^* \dot{y} \frac{\partial \dot{x}}{\partial x} + \frac{D_c \dot{x}}{x + D_c} \frac{\partial \dot{x}}{\partial z} + \delta^* \frac{\dot{x} \dot{y}}{x + D_c} \right] = - \frac{D_c}{x + D_c} \frac{\partial \Pi}{\partial z} \\ &+ \frac{1}{1 + \lambda} \cdot \frac{1}{(x + D_c)^2} \frac{\partial}{\partial x} \left[(x + D_c)^2 \left(1 + \lambda_1^* \left(\delta^* \dot{y} \frac{\partial}{\partial x} + \frac{D_c \dot{x}}{x + D_c} \frac{\partial}{\partial z} \right) \right) \times \left(\frac{\partial \dot{x}}{\partial x} + \delta^* \varepsilon^2 \frac{D_c}{x + D_c} \frac{\partial \dot{y}}{\partial z} - \frac{\dot{x}}{x + D_c} \right) \right] \\ &+ \frac{2 \varepsilon^2}{1 + \lambda} \cdot \frac{D_c}{x + D_c} \frac{\partial}{\partial z} \left[\left(1 + \lambda_1^* \left(\delta^* \dot{y} \frac{\partial}{\partial x} + \frac{D_c \dot{x}}{x + D_c} \frac{\partial}{\partial z} \right) \right) \times \left(\frac{D_c}{x + D_c} \frac{\partial \dot{x}}{\partial z} + \delta^* \frac{\dot{y}}{x + D_c} \right) \right] - \frac{D_0^2}{\mu} \sigma B_0^2 \dot{x} \end{aligned}$$

$$\begin{aligned}
 R_e \varepsilon \left[\frac{\partial \dot{x}}{\partial \xi} + \delta^* \left(y \frac{\partial \dot{x}}{\partial x} + \frac{\dot{x} y}{x + D^*} \right) + \frac{D_c \dot{x}}{x + D_c} \frac{\partial \dot{x}}{\partial z} \right] &= -\frac{D_c}{x + D_c} \frac{\partial \Pi}{\partial z} \\
 + \frac{1}{1 + \lambda} \cdot \frac{1}{(x + D_c)^2} \frac{\partial}{\partial x} \left[(x + D_c)^2 \left(1 + \lambda_1^* \left(\delta^* v \frac{\partial}{\partial x} + \frac{D_c \dot{x}}{x + D_c} \frac{\partial}{\partial x} \right) \right) \times \left(\frac{\partial \dot{x}}{\partial x} + \delta^* \varepsilon^2 \frac{D_c}{x + D_c} \frac{\partial y}{\partial z} - \frac{\dot{x}}{x + D_c} \right) \right] & \quad (2.11) \\
 + \frac{2\varepsilon^2}{1 + \lambda} \cdot \frac{D_c}{x + D_c} \frac{\partial}{\partial z} \left[\left(1 + \lambda_1^* \left(\delta^* y \frac{\partial}{\partial x} + \frac{D_c \dot{x}}{x + D_c} \frac{\partial}{\partial z} \right) \right) \times \left(\frac{D_c}{x + D_c} \frac{\partial \dot{x}}{\partial z} + \delta^* \frac{y}{x + D_c} \right) \right] & - M^2 \dot{x}
 \end{aligned}$$

$$\begin{aligned}
 \frac{\rho c_p \dot{x}_0 D_0^2}{K l_0} \left[\frac{\partial \Theta}{\partial \xi} + \delta^* y \frac{\partial \Theta}{\partial x} + \frac{D_c \dot{x}}{x + D_c} \frac{\partial \Theta}{\partial z} \right] &= \frac{1}{x + D_c} \left[\frac{\partial}{\partial x} \left((x + D_c) \frac{\partial \Theta}{\partial x} \right) + \frac{D_0^2}{l_0^2} \frac{\partial}{\partial z} \left(\frac{D_c}{x + D_c} \frac{\partial \Theta}{\partial z} \right) \right] \\
 + \frac{\mu \dot{x}_0^2}{D_0^2 (\tau_1 - \tau_0)} \cdot \frac{1}{K} \left[4 \cdot \frac{\delta^* D_0^2}{l_0^2} \left(\frac{\partial y}{\partial x} \right)^2 + \left(\frac{\partial \dot{x}}{\partial x} + \delta^* \varepsilon^2 \frac{D_c}{x + D_c} \frac{\partial y}{\partial z} - \frac{\dot{x}}{x + D_c} \right)^2 \right] & \\
 R_e \varepsilon P_r \left[\frac{\partial \Theta}{\partial \xi} + \delta^* y \frac{\partial \Theta}{\partial x} + \frac{D_c \dot{x}}{x + D_c} \frac{\partial \Theta}{\partial z} \right] &= \frac{1}{x + D_c} \left[\frac{\partial}{\partial x} \left((x + D_c) \frac{\partial \Theta}{\partial x} \right) + \varepsilon^2 \frac{\partial}{\partial z} \left(\frac{D_c}{x + D_c} \frac{\partial \Theta}{\partial z} \right) \right] \\
 + B_r \left[4 \delta^* \varepsilon^2 \left(\frac{\partial y}{\partial x} \right)^2 + \left(\frac{\partial \dot{x}}{\partial x} + \delta^* \varepsilon^2 \frac{D_c}{x + D_c} \frac{\partial y}{\partial z} - \frac{\dot{x}}{x + D_c} \right)^2 \right] & \quad (2.12)
 \end{aligned}$$

$$\begin{aligned}
 \frac{D_0^2 u_0}{l_0 D} \left(\frac{\partial n}{\partial \xi} + \delta^* y \frac{\partial n}{\partial x} + \frac{D_c \dot{x}}{x + D_c} \frac{\partial n}{\partial z} \right) &= \frac{1}{x + D_c} \left[\frac{\partial}{\partial x} \left((x + D_c) \frac{\partial n}{\partial x} \right) + \varepsilon^2 \frac{\partial}{\partial z} \left(\frac{D_c^2}{x + D_c} \frac{\partial n}{\partial z} \right) \right] \\
 + \frac{K_\tau (\tau_1 - \tau_0)}{\tau_m (X_1 - X_0)} \cdot \frac{1}{x + D_c} \left[\frac{\partial}{\partial x} \left((x + D_c) \frac{\partial \Theta}{\partial x} \right) + \varepsilon^2 \frac{\partial}{\partial z} \left(\frac{D_c^2}{x + D_c} \frac{\partial \Theta}{\partial z} \right) \right] & \\
 R_e \varepsilon S_c \left[\frac{\partial n}{\partial \xi} + \delta^* y \frac{\partial n}{\partial x} + \frac{D_c \dot{x}}{x + D_c} \frac{\partial n}{\partial z} \right] &= \frac{1}{x + D_c} \left[\frac{\partial}{\partial x} \left((x + D_c) \frac{\partial n}{\partial x} \right) + \varepsilon^2 \frac{\partial}{\partial z} \left(\frac{D_c^2}{x + D_c} \frac{\partial n}{\partial z} \right) \right] \\
 + \frac{S_r S_c}{x + D_c} \left[\frac{\partial}{\partial x} \left((x + D_c) \frac{\partial \Theta}{\partial x} \right) + \varepsilon^2 \frac{\partial}{\partial z} \left(\frac{D_c^2}{x + D_c} \frac{\partial \Theta}{\partial z} \right) \right] & \quad (2.13)
 \end{aligned}$$

where $P_r = \frac{c_p \mu}{K}$ is Prandtl number $R_e = \frac{\rho \dot{x}_0 D_0}{\mu}$ is Reynolds number, $E_c = \frac{\dot{x}_0^2}{c_p (\tau_1 - \tau_0)}$ is Eckert number, $D_c = \frac{D^*}{D_0}$ is the curvature parameter, $S_r = \frac{\rho D K_\tau (\tau_1 - \tau_0)}{\mu (X_1 - X_0) \tau_m}$ is Soret number, $B_r = P_r E_c$ is Brickmann number, $S_c = \frac{\mu}{D_p}$ is Schmidt number, $M = B_0 D_0 \left(\frac{\sigma}{\mu} \right)^{\frac{1}{2}}$ is Hartmann number, where B_0 is the external constant magnetic field in the radial direction, $\lambda^* = \frac{\lambda_1 \dot{x}_0}{l_0}$. Now, we make the equations simpler for low grade by deducing the two requirements, stenosis $\delta^* = \frac{\delta}{D_0} \ll 1$ and $\varepsilon = \frac{D_0}{l_0} \approx o(1)$. For a low Reynolds number flow, in the annulus with mild stenosis, the radial velocity is negligibly tiny and can be disregarded. With these assumptions, equations (2.9)-(2.13) become

$$\frac{\partial \dot{x}}{\partial z} = 0 \quad (2.14)$$

$$\frac{\partial \Pi}{\partial x} = 0 \quad (2.15)$$

$$D_c (1 + \lambda) (x + D_c) \frac{\partial \Pi}{\partial z} = (x + D_c)^2 \frac{\partial^2 \dot{x}}{\partial x^2} + (x + D_c) \frac{\partial \dot{x}}{\partial x} - M^2 \dot{x} \quad (2.16)$$

$$\frac{\partial}{\partial r} \left((x+D_c) \frac{\partial \Theta}{\partial r} \right) = -B_r \left(\frac{\partial \dot{x}}{\partial r} - \frac{\dot{x}}{x+D_c} \right)^2 \quad (2.17)$$

$$\frac{\partial}{\partial x} \left((x+D_c) \frac{\partial n}{\partial x} \right) = -S_r S_c \frac{\partial}{\partial r} \left((x+D_c) \frac{\partial \Theta}{\partial x} \right). \quad (2.18)$$

The boundary conditions are

$$\dot{x} = 0, \quad \Theta = 0, \quad n = 0 \quad \text{on} \quad x = \varepsilon, \quad (2.19)$$

$$\dot{x} = 0, \quad \Theta = 1, \quad n = 1 \quad \text{on} \quad x = D(z). \quad (2.20)$$

$$D(z) = \begin{cases} 1 + \frac{\delta^*(z-s^*)}{3} [32(z-s^*)^3 - 96(z-s^*)^2 + 94(z-s^*) - 33], & s^* \leq z \leq s^* + \frac{3}{2} \\ 1, & \text{otherwise} \end{cases}$$

$$\text{where } s^* = \frac{s}{l_0}, \quad \varepsilon = \frac{\bar{a}}{D_0}.$$

Applying the boundary conditions (2.19)-(2.20) for the expressions of axial velocity, temperature, and concentration (2.14)-(2.18) to get

$$\dot{x} = F_1(x+D_c)^M + F_2(x+D_c)^{-M} + \frac{1}{1-M^2} \left\{ D_c(1+\lambda)(x+D_c) \frac{d\Pi}{dz} \right\} \quad (2.21)$$

$$\Theta = -B_r \left[\frac{(M-1)^2}{(2M-1)^2} F_1^2(x+D_c)^{2M-1} + \frac{(M+1)^2}{(3-2M)^2} F_2^2(x+D_c)^{3-2M} - 2(M^2-1)F_1F_2(x+D_c)^{-1} \right]$$

$$n = -B_r S_r S_c \left[\frac{(M-1)^2}{(2M-1)^2} F_1^2(x+D_c)^{2M-1} + \frac{(M+1)^2}{(3-2M)^2} F_2^2(x+D_c)^{3-2M} - 2(M^2-1)F_1F_2(x+D_c)^{-1} \right]$$

where the functions $F_1(z), F_2(z)$ are given by

$$F_1 = \frac{(D+D_c)^M(\varepsilon+D_c)^M}{(\varepsilon+D_c)^{2M} - (D+D_c)^{2M}} \left[\frac{1}{1-M^2} \left\{ D_c(1+\lambda) \frac{d\Pi}{dz} ((\varepsilon+D_c)(D+D_c)^M - (\varepsilon+D_c)^M(D+D_c)) \right\} \right]$$

$$F_2 = \frac{(\varepsilon+D_c)^M(D+D_c)^M}{(D+D_c)^{2M} - (\varepsilon+D_c)^{2M}} \left[\frac{1}{1-M^2} \left\{ D_c(1+\lambda) \frac{d\Pi}{dz} ((\varepsilon+D_c)^M(D+D_c) - (\varepsilon+D_c)(D+D_c)^M) \right\} \right].$$

Here, the wall shear stress distribution can be expressed using equation (2.21)

$$W_s = \left[F_1 M(x+D_c)^{M-1} - F_2 M(x+D_c)^{-M-1} + \frac{1}{1-M^2} \left\{ D_c(1+\lambda) \frac{d\Pi}{dz} \right\} - \frac{F_1(x+D_c)^M + F_2(x+D_c)^{-M} + \frac{1}{1-M^2} \left\{ D_c(1+\lambda)(x+D_c) \frac{d\Pi}{dz} \right\}}{x+D_c} \right].$$

The stream function is

$$\psi = - \left[\frac{F_1}{M+1} ((x+D_c)^{M+1} + (\varepsilon+D_c)^{M+1}) + \frac{F_2}{1-M} ((x+D_c)^{1-M} + (\varepsilon+D_c)^{1-M}) + \frac{1}{1-M^2} \left\{ D_c(1+\lambda) \frac{d\Pi}{dz} \left(\frac{(x+D_c)^2}{2} + \frac{(\varepsilon+D_c)^2}{2} \right) \right\} \right].$$

The fluid flow rate is

$$V = \int_{\varepsilon}^D \dot{x} dx$$

$$V = \frac{F_1}{M+1} [(D+D_c)^{M+1} - (\varepsilon+D_c)^{M+1}] + \frac{F_2}{1-M} [(D+D_c)^{1-M} - (\varepsilon+D_c)^{1-M}] + \frac{1}{1-M^2} \left\{ D_c(1+\lambda) \frac{d\Pi}{dz} \left(\frac{(D+D_c)^2}{2} - \frac{(\varepsilon+D_c)^2}{2} \right) \right\}.$$

The arterial pressure drop is given in the form of

$$\Delta\Pi = \int_0^{L^*} \left(-\frac{d\Pi}{dz} \right) dz.$$

The resistance impedance expression

$$\Lambda = \frac{\Delta\Pi}{V}$$

$$\Lambda = \frac{2(1-M)^2}{D_c(1+\lambda)V[(D+D_c)^2 - (\varepsilon+D_c)^2]} \left[\frac{V-F_1}{M+1} ((D+D_c)^{M+1} - (\varepsilon+D_c)^{M+1}) - \frac{F_2}{1-M} ((D+D_c)^{1-M} - (\varepsilon+D_c)^{1-M}) \right] L^*$$

where $L^* = \frac{L}{l_0}$.

3. Results

This section shows the graphical outcomes for the different parameter, so here we study the many characteristics of blood flow across overlapping stenosed arteries with heat, mass transport, and magnetic field by charting the figures of axial velocity \dot{x} , wall shear stress W_s , flow rate V , impedance resistance Λ , temperature profile Θ and concentration n . Various graphs are drawn for the different possible values of the parameters like - height of the stenosis, Hartmann number, Brickmann number, Soret number, and Schmidt number, etc.

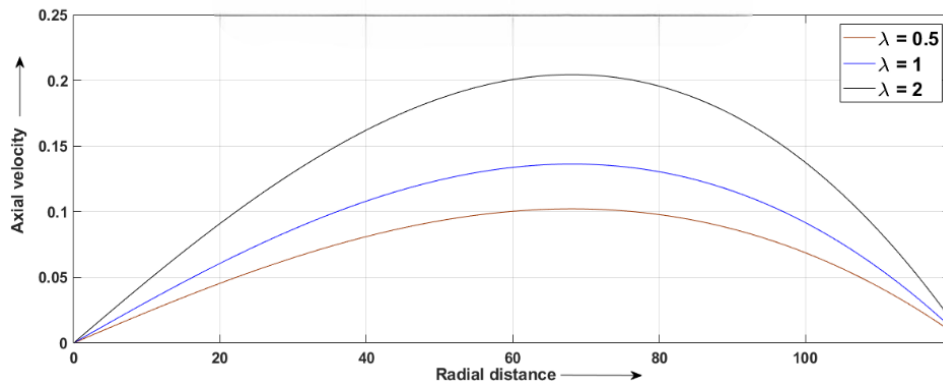


Figure 3.1. Axial velocity with different Jeffery parameter

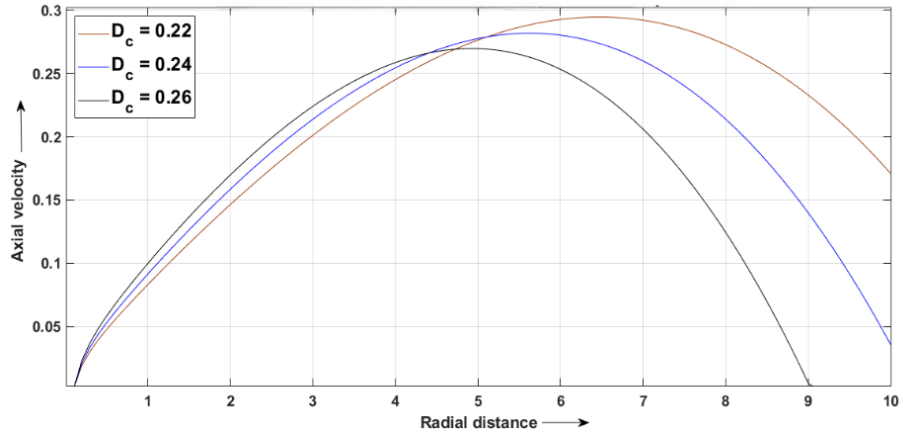


Figure 3.2. Axial velocity for different values of curvature parameter

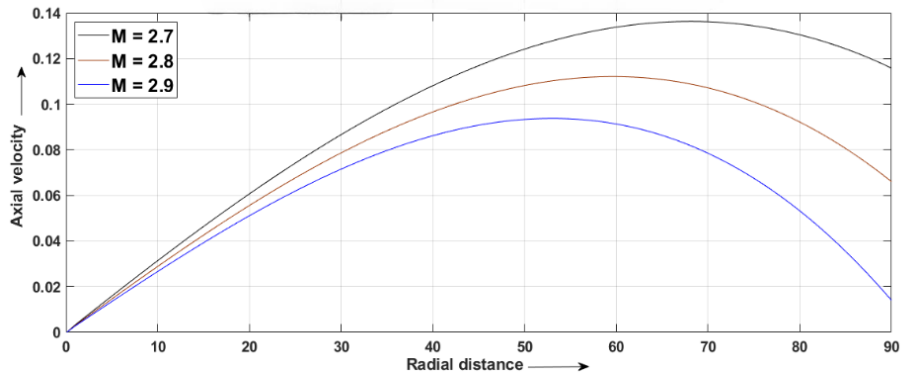


Figure 3.3. Axial velocity for different values of Hartmann number

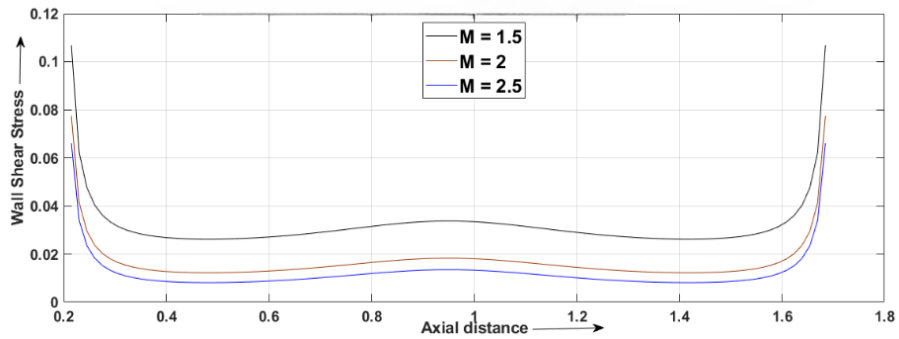


Figure 3.4. Wall shear stress distribution for different values of Hartmann number

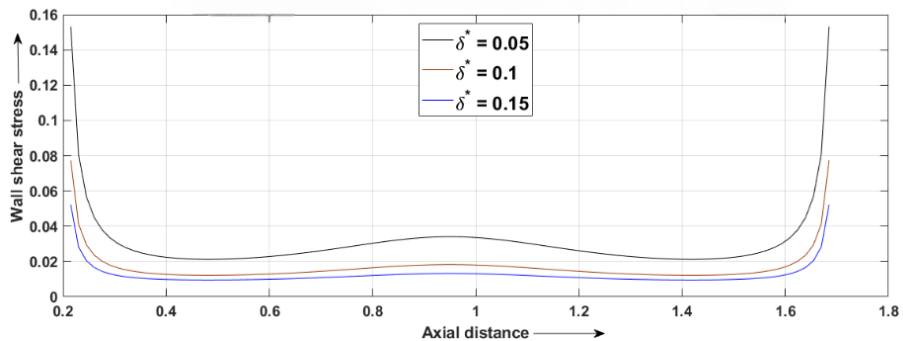


Figure 3.5. Wall shear stress distribution for different values of critical height

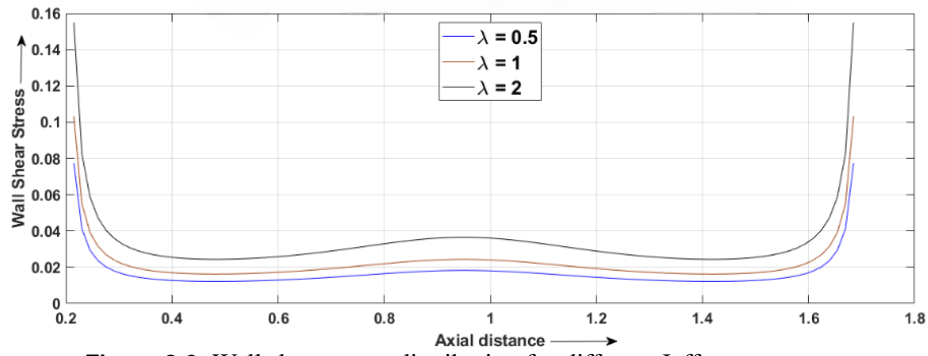


Figure 3.6. Wall shear stress distribution for different Jeffery parameters

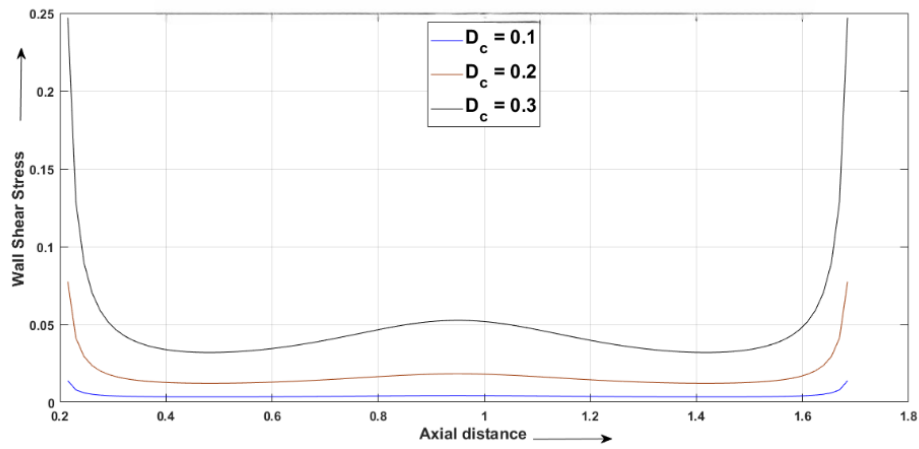


Figure 3.7. Wall shear stress distribution for different values of curvature parameter

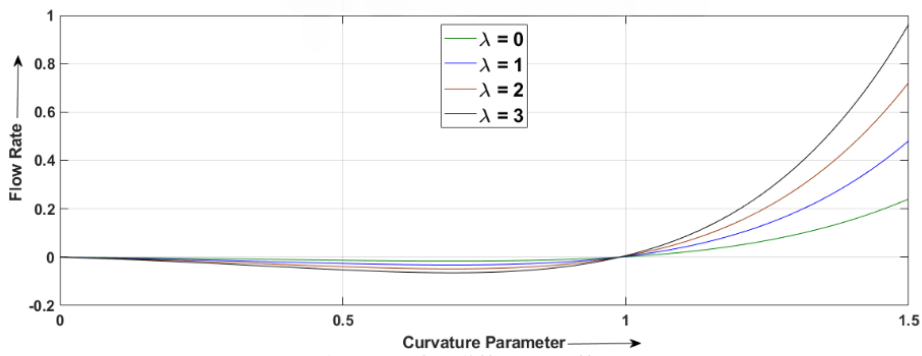


Figure 3.8. Flow rate for different Jeffery parameters

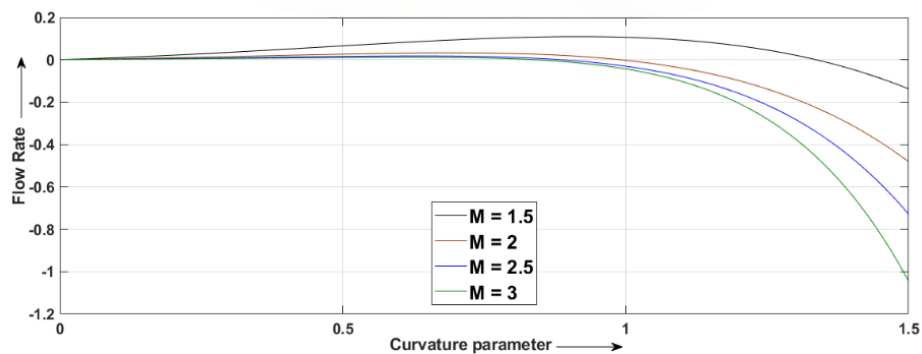


Figure 3.9. Flow rate for different Hartmann numbers

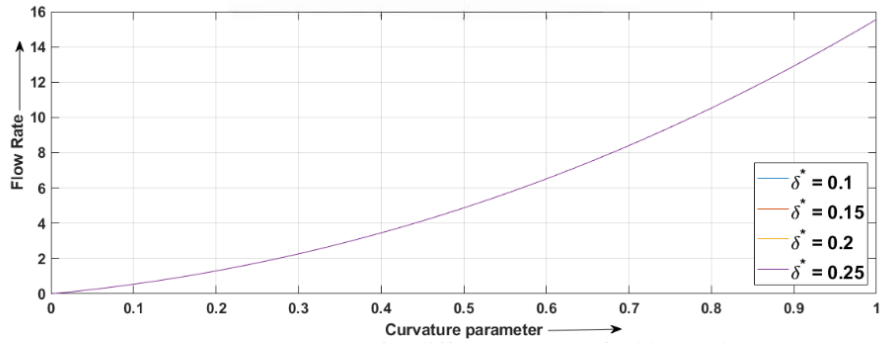


Figure 3.10. Flow rate for different values of critical height

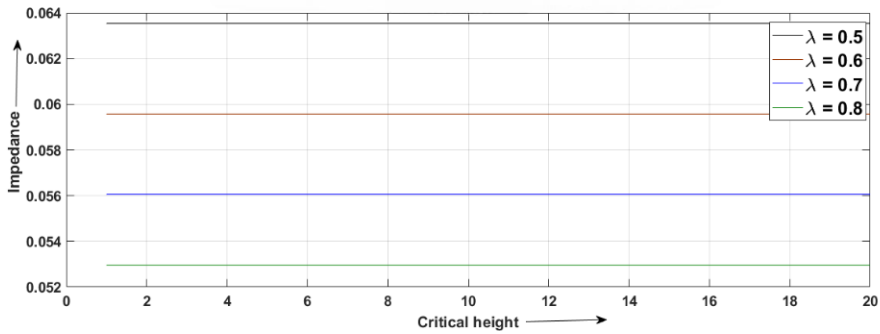


Figure 3.11. Graph of impedance for different Jeffery parameters

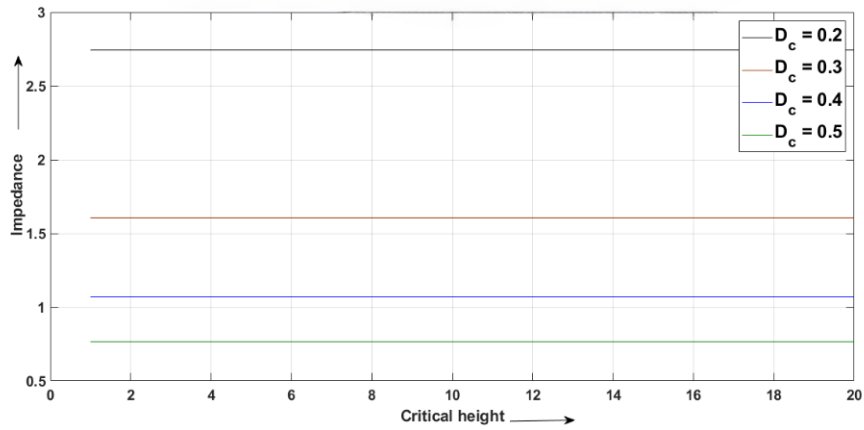


Figure 3.12. Graph of impedance for different values of curvature parameter

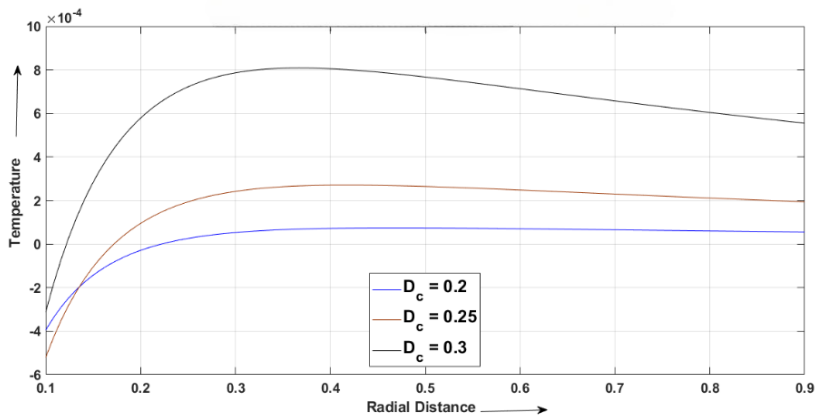


Figure 3.13. Temperature for different curvature parameters

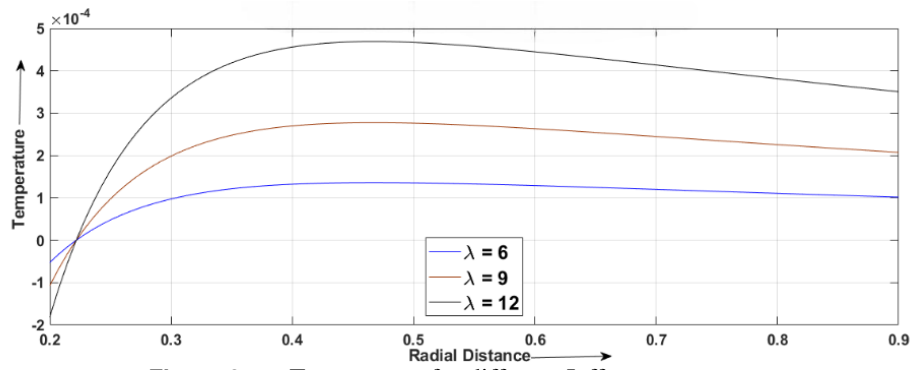


Figure 3.14. Temperature for different Jeffery parameters

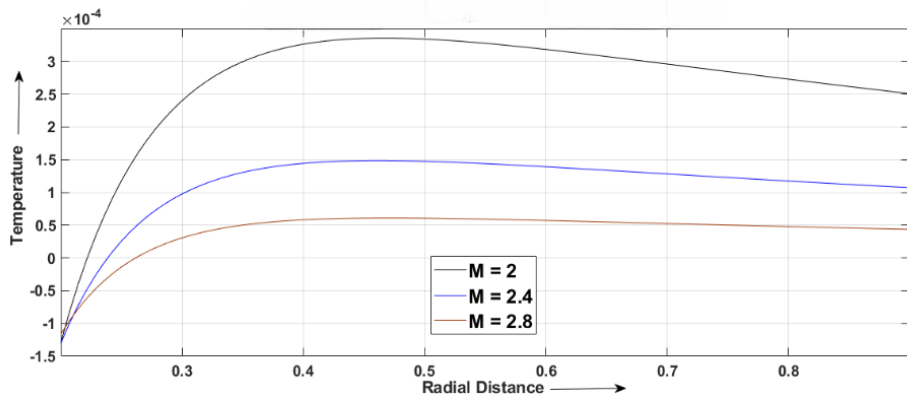


Figure 3.15. Temperature for different Hartmann numbers

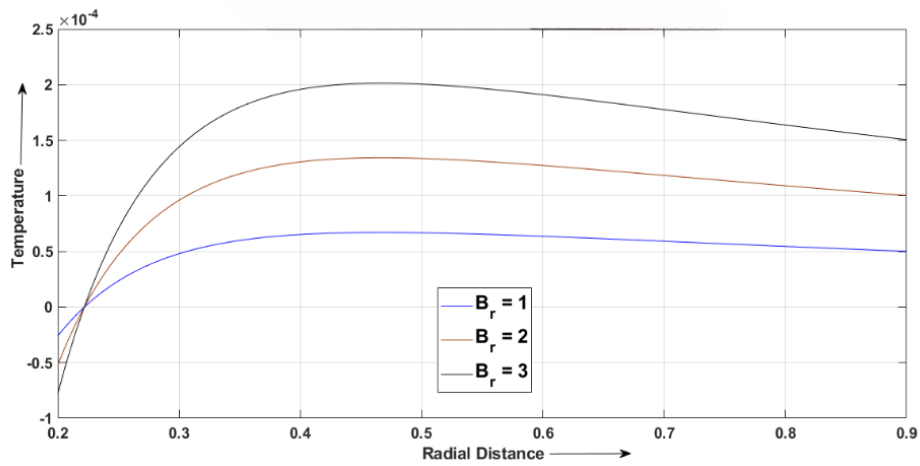


Figure 3.16. Temperature for different Brickmann numbers

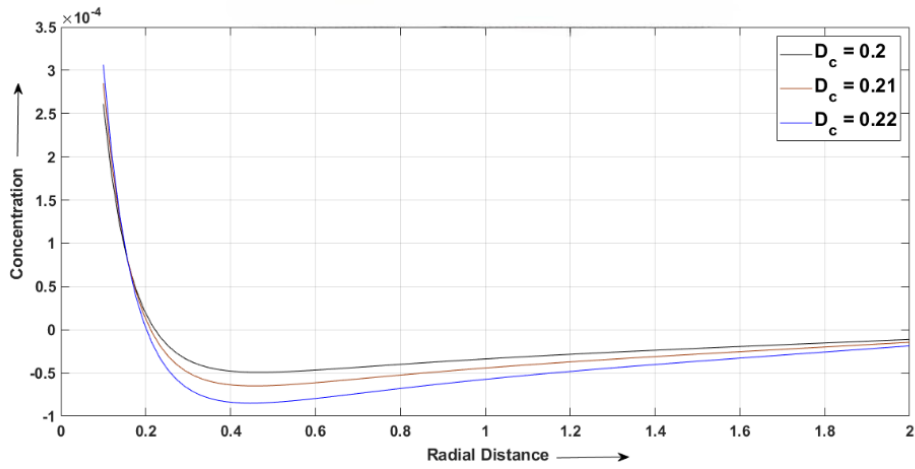


Figure 3.17. Concentration for different curvature parameters

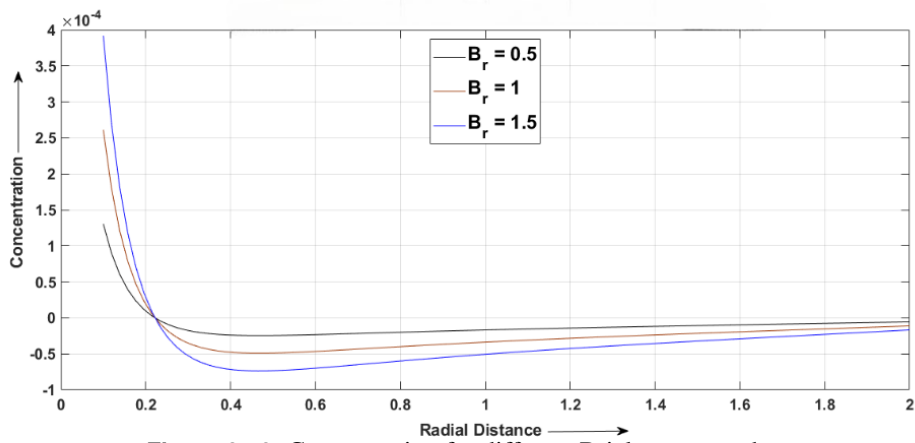


Figure 3.18. Concentration for different Brinkmann number

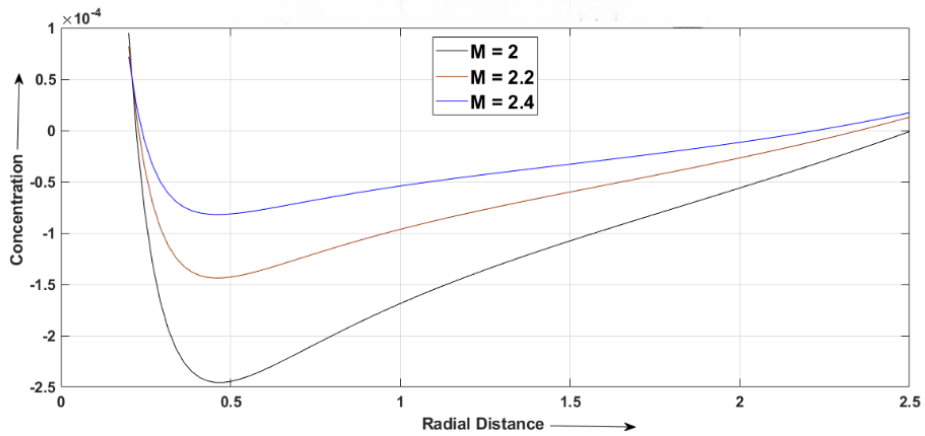


Figure 3.19. Concentration for different Hartmann numbers

We have generated figures to illustrate the effects of the Jeffrey parameter, curvature parameter, and Hartmann number on axial velocity. The results indicate that an increase in both the curvature and Jeffrey parameters leads to an enhancement in axial velocity. This rise in axial velocity suggests that higher viscoelasticity contributes positively to blood flow, potentially reducing the risk of thrombosis. Conversely, an increase in the Hartmann number results in a decrease in axial velocity, implying that the applied magnetic field impedes blood flow.

The plotted figures also depict the distribution of wall shear stress in the region of a bent stenosed artery. It is observed that wall shear stress increases with rising values of the Jeffrey and curvature parameters. However, an inverse relationship is noted with the Hartmann number, and critical height both contribute to a reduction in wall shear stress.

Regarding flow rate, variations with the curvature parameter for different values of critical height, Hartmann number, and Jeffrey parameter reveal that flow rate increases with higher Jeffrey parameter and critical height. In contrast, an increase in the Hartmann number leads to a decline in flow rate. Since an adequate flow rate helps prevent blood pooling, this finding highlights the significance of parameter tuning in maintaining healthy circulation.

The figures also demonstrate how impedance varies in this context. Impedance is found to decrease with increasing curvature parameter but increases with a higher Jeffrey parameter.

Temperature distribution with respect to radial distance is also analyzed for various values of the curvature parameter, Jeffrey parameter, Hartmann number, and Brinkman number. The results show that temperature increases with higher curvature parameter, Jeffrey parameter, and Brinkman number, whereas an increase in the Hartmann number leads to a decrease in temperature.

Finally, concentration profiles are shown for varying values of the Hartmann number, Brinkman number, and curvature parameter. The concentration decreases with increases in the curvature parameter and Brinkman number, while a higher Hartmann number corresponds to an increase in concentration.

4. Conclusion

Jeffrey fluid is a type of non-Newtonian fluid that is significantly used in certain applications as it involves viscous and elastic behaviors, contrary to the Newtonian model, this model considers the relaxation and retardation times, therefore the fluid has a slow response to changes. Thus, Jeffrey's model examines the mass and heat transfer in blood flow that is catalyzed by a magnetic field. The trapping phenomenon occurs when an accumulation of blood is caught inside a closed loop of flow, moving along with the main blood, but staying separate. We talk about how different parameters affect temperature, concentration, flow rate, wall shear stress, axial velocity, and resistance to flow.

The main observations are as follows.

1. As a result of the successive increase in Jeffrey parameter the axial velocity, wall shear stress, flow rate, and temperature increase.
2. The values of axial velocity, temperature, and wall shear stress increase with increasing curvature parameter, while the inverse effect is observed in concentration.
3. The increase in magnetic field parameter, i.e., Hartmann number, escalates the concentration, whereas flow rate, wall shear stress, axial velocity, and temperature decline.
4. As the critical height increases, both the flow rate and the shear stress decrease.
5. As the Brinkman number increases, the flow rate increases, while the concentration reduces.

5. Article Information

Acknowledgements: The authors express their sincere thanks to the editor and the anonymous reviewers for their helpful comments and suggestions.

Author's Contributions: **G.S.:** Methodology, investigations, software implementation, visualization, and writing. **S. K. A.:** Conceptualization, formal analysis, original draft preparation, validation, review, and editing. All authors read and approved the final manuscript.

Artificial Intelligence Statement: Artificial intelligence techniques were employed in this study to assist in specific tasks, e.g., language correction, some forgotten commands used in Latex.

Conflict of Interest Disclosure: The authors declare that there is no conflict of interest.

Plagiarism Statement: This article was scanned by the plagiarism program.

References

- [1] H. Schlichting, *Boundary Layer Theory*, McGraw Hill Education Indian Edition 2014, ISBN-13:978-93-329-0282-4, 7th Edition.
- [2] S. Chakravarty, *Effect of stenosis on the flow behavior of blood in an artery*, Int. J. Eng. Sci., **25**(8) (1987), 1003-1016. [https://doi.org/10.1016/0020-7225\(87\)90093-0](https://doi.org/10.1016/0020-7225(87)90093-0)
- [3] M. S. Shabbir, N. Ali, Z. Abbas, *Unsteady blood flow of non-Newtonian fluid through a rigid artery in the presence of multi-irregular stenoses*. J. Braz. Soc. Mech. Sci. Eng., **40** (2018), Article ID 413. <https://doi.org/10.1007/s40430-018-1327-x>
- [4] R. Padma, P. Ponalagusamy, R. T. Selvi, *Mathematical modeling of electro hydrodynamic non-Newtonian fluid flow through tapered arterial stenosis with periodic body acceleration and applied magnetic field*, Appl. Math. Comput., **362** (2019), Article ID 124453. <https://doi.org/10.1016/j.amc.2019.05.024>
- [5] R. K. Dash, G. Jayaraman, K. N. Mehta, *Flow in a catheterized curved artery with stenosis*, J. Biomech., **32**(1) (1999), 49-61. [https://doi.org/10.1016/S0021-9290\(98\)00142-0](https://doi.org/10.1016/S0021-9290(98)00142-0)
- [6] M. Ayub, I. Shahzadi, S. Nadeem, *A ballon model analysis with Cu-blood medicated nanoparticles as drug agent through overlapped curved stenotic artery having compliant walls*, Microsyst. Technol., **25** (2019), 2949-2962. <https://doi.org/10.1007/s00542-018-4263-x>
- [7] A. Zaman, A. A. Khan, *Time dependent non-Newtonian nano-fluid (blood) flow in w-shape stenosed channel; with curvature effects*, Math. Comput. Simul., **181** (2021), 82-97. <https://doi.org/10.1016/j.matcom.2020.09.017>
- [8] A. Ahmed, S. Nadeem, *Shape effect of Cu-nanoparticles in unsteady flow through curved artery with catheterized stenosis*, Results Phys., **7** (2017), 677-689. <https://doi.org/10.1016/j.rinp.2017.01.015>
- [9] A. Zaman, N. Ali, M. Sajid, *Slip effects on unsteady non-Newtonian blood flow through an inclined catheterized overlapping stenotic artery*, AIP Adv., **6**(1) (2016), Article ID 015118. <https://doi.org/10.1063/1.4941358>
- [10] T. Hayat, N. Ali, S. Asghar, *An analysis of peristaltic transport for flow of a Jeffrey fluid*, Acta Mech., **193** (2007), 101-112. <https://doi.org/10.1007/s00707-007-0468-2>
- [11] S. Chakravarty, P. K. Mandal, *A Nonlinear two-dimensional model of blood flow in an overlapping arterial stenosis subjected to body acceleration*, Math. Comput. Model., **24**(1) (1996), 43-58. [https://doi.org/10.1016/0895-7177\(96\)00079-9](https://doi.org/10.1016/0895-7177(96)00079-9)
- [12] M. A. El Kot, *Theoretical simulation of blood flow for non-Newtonian Fluid through diseased catheterized curved artery with heat and mass transfer*, (2024), 12 pages. <https://doi.org/10.22541/au.170665633.35943336/v1>